2nd URSI AT-RASC, Gran Canaria, 28 May - 1 June 2018

Determining Installation Errors for DOA Estimation with Four-Quadrant Monopulse Arrays by using Installed Element Patterns

Henrik Frid[(1)], and B. L. G. Jonsson[(2)]
(1) Saab Surveillance and KTH Royal Institute of Technology. E-mail: henrik.frid@ee.kth.se
(2) KTH Royal Institute of Technology, Osquldas väg 10, SE-10044 Stockholm, Sweden.

Abstract

The four-quadrant monopulse array is widely used for direction of arrival (DOA) estimation. Errors in the angle estimate are introduced when installing the array on a platform, due to unwanted reflections in the platform, as well as reflection and refraction in the radome. These installation effects are captured in the installed element patterns, which can be computed using a number of computational electromagnetics methods. In this paper, we demonstrate that the error introduced in the DOA estimate can be determined from the installed element patterns. To illustrate how the method is used, we present results for two cases: (a) BoR-array without radome and (b) BoR-array with an extended hemispherical radome. The presented method can be applied for any installation configuration, as long as the installed element patterns can be computed.

1 Introduction

Several remote sensing systems require the capability to determine the direction to a radiation source. This is referred to as direction of arrival (DOA) estimation. The monopulse method [1, 2] enables accurate DOA estimation using the classical four-quadrant array configuration, as illustrated in Figure 1. The radiation source of interest can be a transmitter, or radiating currents on a target due to illumination by a radar. Hence, the monopulse method is commonly used both in active systems, which consist of both a transmitter and a receiver (e.g. radar), and passive systems which consists only of a receiver (e.g. electronic support measures). The monopulse method is also relatively robust against both unintentional and intentional interference (jamming), see e.g. [3].

To estimate system performance for a four-quadrant monopulse array installed on a platform (such as an aircraft, satellite or automotive vehicle), one needs to take installation effects into account. The most important installation effects are (I) reflections in the platform, which cause multipath errors and "ripple" in the antenna far-fields, and (II) reflections and refraction in the radome. Some attention has previously been given to radome-induced pointing error [4], as well as increased side-lobe levels due to radome installation [5].

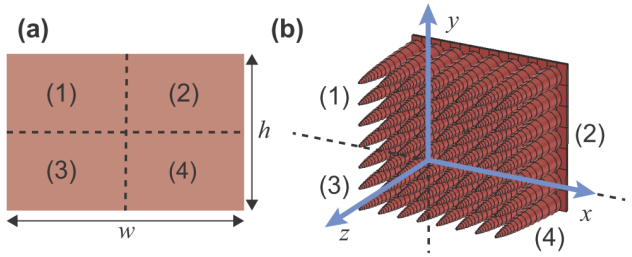

Figure 1. (a) Illustration of array aperture of dimensions $w \times h$ divided into four sub-arrays of dimensions $w/2 \times h/2$. The sub-array numbering is shown. (b) BoR-array antenna divided into corresponding sub-arrays.

Computing the installed antenna pattern for an antenna installed on a platform is a computationally heavy problem due to the large size of the structure in terms of wavelengths [6, 7]. With modern hardware and advanced computational methods such as [8], it is now possible to compute the installed antenna patterns even for very large platforms at gigahertz frequencies. The computed installed antenna patterns can be used to determine system performance in terms of angular coverage, side-lobe level and cross-polarization. It has recently been shown that the installed antenna patterns also can be used to estimate the isolation between antennas installed on the same platform [7]. In this paper, we show that the installed antenna patterns can be used to determine the installation effects on the accuracy of a four-quadrant monopulse system.

The paper is organized as follows. The method for determining the installation error is presented in Section 2. Section 3 presents results for two cases: (a) BoR-array without radome and (b) BoR-array with an extended hemispherical radome. Finally conclusions are presented in Section 4.

2 Theory

We start with a brief review of the background theory [1] of monopulse DOA estimation with four-quadrant array antennas in Section 2.1. The purpose of this is to show which errors occur in the estimation. We introduce an error term ε to model these errors. Based on this, a method to determine installation errors is presented in Section 2.2. The

presented method uses the installed element patterns (IEPs) to determine the installation errors.

2.1 Four-quadrant monopulse arrays

We are interested in estimating $\hat{r} = u(\theta,\phi)\hat{x} + v(\theta,\phi)\hat{y} + \cos(\theta)\hat{z}$, which is the direction to the radiation source with respect to the system of coordinates in Figure 1. Let s_1, s_2, s_3 and s_4 be the signals received simultaneously by the sub-arrays with the corresponding index. The sum s, elevation difference d_e and azimuth difference d_a are defined as $s = s_1 + s_2 + s_3 + s_4$, $d_e = s_1 + s_2 - s_3 - s_4$ and $d_a = s_1 - s_2 + s_3 - s_4$. The measured elevation difference signal due to an incident plane wave, with amplitude a and unit polarization $\hat{n}$, is determined by

$$d_e(\hat{r}) = a\hat{n}\cdot\Big[C_1\vec{f}_1^{(v)}(\hat{r})e^{jk\vec{r}_1\cdot(\hat{r}-\hat{r}_0)} + C_2\vec{f}_2^{(v)}(\hat{r})e^{jk\vec{r}_2\cdot(\hat{r}-\hat{r}_0)} - C_3\vec{f}_3^{(v)}(\hat{r})e^{jk\vec{r}_3\cdot(\hat{r}-\hat{r}_0)} - C_3\vec{f}_4^{(v)}(\hat{r})e^{jk\vec{r}_4\cdot(\hat{r}-\hat{r}_0)}\Big], \quad (1)$$

where $\vec{f}_i^{(v)}$ is the vector far-field amplitude of sub-array i and $k = 2\pi/\lambda$. A progressive phase or time delay distribution over the array aperture is assumed to steer the main lobe in the sum pattern in the direction $\hat{r}_0 = u_0\hat{x} + v_0\hat{y} + \cos(\theta_0)\hat{z}$. Eqn. (1) is valid when the far-field amplitudes are normalized following [7]. The frequency-dependent coefficients C_i describe the receiving properties such as loss, low-noise amplification and mismatch. The monopulse receiver should be carefully designed such that these coefficients are equal, i.e. $C_i \approx C$. Furthermore, we require the sub-arrays to be equal, i.e. of equal size and tapering. We can therefore introduce the following notation:

$$Ca\hat{n}\cdot\vec{f}_i^{(v)}(\hat{r}) = f(\hat{r}) + \varepsilon(\hat{r}), \quad (2)$$

where we have introduced the error term $\varepsilon(\hat{r})$. This error term includes the following effects:

(i) The sub-array far-field amplitudes $\vec{f}_i^{(v)}$ are not exactly equal, since they are subject to different edge-effects. Furthermore, it is usually of interest to taper the sub-arrays differently in order to suppress the side-lobe level, see e.g. [5].

(ii) The far-field amplitudes $\vec{f}_i^{(v)}$ can also include installation effects, e.g. reflection and refraction in the radome, and reflections in platform.

(iii) There can be some non-ideal performance of the array feed network, whereby there is some error in the approximation $C_i \approx C$.

The method presented in Section 2.2 can be used to study the effects of (i) and (ii).

The classical derivation for DOA estimation below assumes the idealized case $\varepsilon(\hat{r}) = 0$. Assume that the phase-center of each sub-array is located in the geometrical center of the corresponding sub-array, i.e. $\vec{r}_1 = -w\hat{x}/4 + h\hat{y}/4$, $\vec{r}_2 = w\hat{x}/4 + h\hat{y}/4$, $\vec{r}_3 = -w\hat{x}/4 - h\hat{y}/4$ and $\vec{r}_4 = w\hat{x}/4 - h\hat{y}/4$. Using Euler's formula, it is now possible to simplify (1):

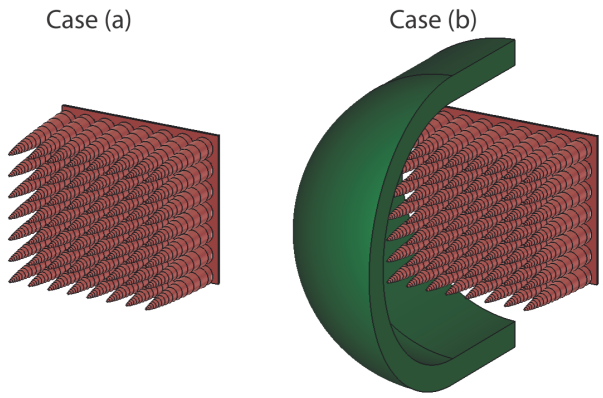

Figure 2. Illustration of the two investigated cases: (a) BoR-array in free space and (b) BoR-array installed behind radome. Half of the radome is hidden to show the array beneath.

$$d_e(\hat{r}) = 4jf(\hat{r})\cos(kw(u-u_0)/4)\sin(kh(v-v_0)/4). \quad (3)$$

The azimuth difference d_a and sum s signals are found by analogy:

$$d_a(\hat{r}) = -4jf(\hat{r})\sin(kw(u-u_0)/4)\cos(kh(v-v_0)/4) \quad (4)$$

$$s(\hat{r}) = 4f(\hat{r})\cos(kw(u-u_0)/4)\cos(kh(v-v_0)/4). \quad (5)$$

The array factors are found from (3)-(5) by omitting the factor $f(\hat{r})$. Note that the difference patterns are odd, with a null in the direction of the main lobe of the sum pattern, i.e. when $(u,\ v) = (u_0,\ v_0)$. The difference array factors have two major lobes, located on opposite sides of this null, with opposite phase. Eqns. (3) and (4) are useful when considering the antenna's installation location on a platform, since it is desirable to avoid illuminating the platform or the ground with the difference lobes, since this results in sensitivity to unwanted reflections. As understood from (3)-(4), this is more difficult at lower frequencies, since the angular separation between the difference lobes grows with decreasing frequency.

By dividing (3) and (4) by (5), we have the following relations[1] between the monopulse ratios and the DOA $(u,\ v)$:

$$\frac{d_e}{s} = j\tan(\kappa_e(v-v_0)) \quad (6)$$

$$\frac{d_a}{s} = -j\tan(\kappa_a(u-u_0)). \quad (7)$$

The advantage of this normalization is that the monopulse ratios are independent of $f(\hat{r})$. However, one should keep in mind that this only holds for the idealized case $\varepsilon = 0$. The monopulse slope coefficients are given by $\kappa_e = kh/4$ and $\kappa_a = kw/4$ for the case of equal sub-arrays. When

[1] A similar relation is found in [1].

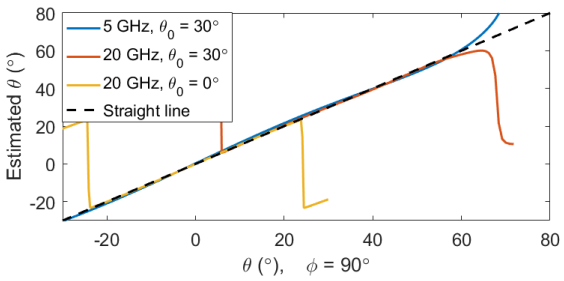

Figure 3. Estimated angle of arrival $\tilde{\theta}$, extracted from simulation data, plotted versus angle of arrival θ. Simulated far-fields for case (a) were used.

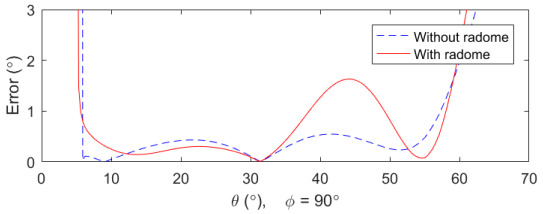

Figure 4. Estimation error in polar angle $|\theta - \tilde{\theta}|$, computed in the elevation plane ($\phi = 90°$) at 20 GHz. The scan angle is set to $\theta_0 = 30°$ in the elevation plane. Both cases (a) and (b) are presented.

tapering is applied in a way where the sub-arrays are not equal, (6)-(7) can still be applied approximately by replacing the monopulse slope coefficients κ_e and κ_a by their corresponding tapered values. By tapering the array excitation, the beamwidth is increased and the monopulse slope coefficients are therefore decreased, see e.g. [5].

In conclusion, the unknowns u and v can be directly determined from the measured monopulse ratios by inverting (6)-(7). Thereafter, θ, ϕ and $\hat{r}$ can be calculated. In principle, this enables the DOA to be estimated from a single measurement, hence the name monopulse. It is common to linearize (6)-(7) under the assumption that $|v - v_0|$ and $|u - u_0|$ are small. Since (6)-(7) are periodic, the estimate of u and v is ambiguous outside the *unambiguous region*:

$$\pi/2 > \begin{cases} \kappa_e |v - v_0| \\ \kappa_a |u - u_0|. \end{cases} \tag{8}$$

In practice, a guard antenna is therefore needed to verify that the measured signal was received within the unambiguous region and not in the side-lobes, see e.g. [9].

2.2 Determining installation errors

To determine the installation error, we will use the installed antenna patterns, which are known from simulation or measurement. The installed elevation differencec pattern, azimuth difference pattern and sum pattern are denoted by $\vec{d}_{e,inst}$, $\vec{d}_{a,inst}$, and $\vec{s}_{inst}$. The monopulse ratios that would be measured for an incident plane wave of unit polarization

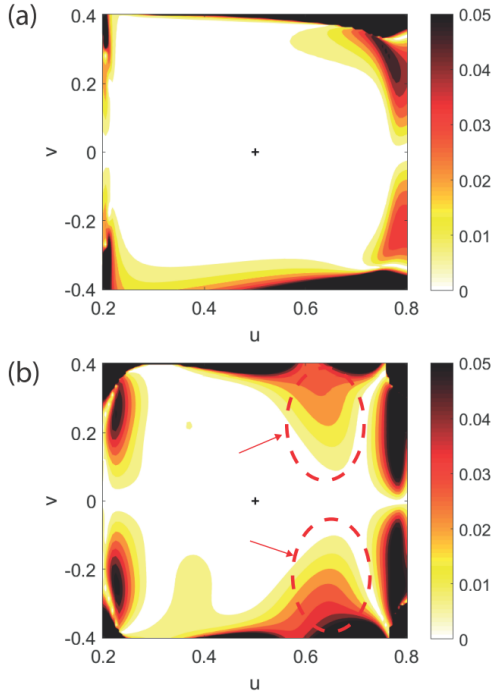

Figure 5. Elevation estimation error $|v - \tilde{v}|$ at 20 GHz for (a) BoR-array without radome and (b) BoR-array with radome. The scan direction $(u_0,\ v_0)$ is marked by $+$. The axis limits are set by (8). Regions of radome-induced pointing error are indicated by red circles and arrows.

$\hat{n}$ can be determined as:

$$(d_e/s)_{inst} = \frac{\hat{n} \cdot \vec{d}_{e,inst}}{\hat{n} \cdot \vec{s}_{inst}} \tag{9}$$

$$(d_a/s)_{inst} = \frac{\hat{n} \cdot \vec{d}_{a,inst}}{\hat{n} \cdot \vec{s}_{inst}}. \tag{10}$$

By inserting (9)-(10) into (6)-(7), we can estimate the DOA for a known direction $(u,\ v)$. The estimated DOA $(\tilde{u},\ \tilde{v})$ will then include the errors (i)-(ii) described in the previous section, since these errors are captured by the installed far-fields. The installation error can thereafter be evaluated as:

$$\text{elevation error } = v - \tilde{v} \tag{11}$$

$$\text{azimuth error } = u - \tilde{u}. \tag{12}$$

This can be repeated for a set of directions $(u,\ v)$, scan directions $(u_0,\ v_0)$, polarization $\hat{n}$ and frequencies. By analyzing the data given by (11)-(12) for these parameter sweeps, we can determine the installed performance of the four-quadrant monopulse array.

3 Results

We present simulation results for a wideband BoR-array antenna of dimensions $w = 50$ mm and $h = 43$ mm, designed for $5 - 24$ GHz. The BoR-array (Figure 1(b)) consists of 8×6 elements of vertical ($\hat{y}$) polarization. The array

is installed behind a radome with an extended hemispherical shape of diameter 90 mm and extension 34 mm, made from quartz ($\varepsilon_r = 3.2, \tan\delta = 0.006$) of thickness 7.5 mm. The active element patterns (AEPs) for the BoR-array were computed using the finite integration technique (FIT) implemented in CST Microwave Studio. We consider two cases: (a) the BoR-array in free space and (b) the BoR-array installed behind the radome. The two cases are illustrated in Figure 2. The AEPs for case (b) are referred to as installed element patterns (IEPs). A post-processing script implemented in Matlab was used to compute the sum and difference far-fields. The errors were thereafter computed using (11)-(12) for both case (a) and case (b). Any combination of frequency, tapering, incident polarization and scan direction can be studied efficiently using this post-processing method. Some representative results are presented below.

As a first example, we estimate the polar angle $\tilde{\theta}$ for a set of angles θ in the elevation plane $\phi = 90^\circ$, for various frequencies and scan angles θ_0. The results for case (a) are shown in Figure 3. As expected, the relation between $\tilde{\theta}$ and θ collapses on a straight line with unity slope. The boundaries of the unambiguous region are visible in the figure. Any deviation from this straight line is due to non-ideal antenna far-fields, as described by (i)-(ii) in Section 2.1. Since the radome is not considered for case (a), the minor deviation seen here is due to (i) and not (ii). Figure 4 shows the estimation error in polar angle, i.e. $|\theta - \tilde{\theta}|$ for both cases (a) and (b). This figure shows that the radome increases the error in the angle estimate in a region between $31^\circ < \theta < 53^\circ$, where a maximum error of 2° occurs. For most applications, this radome-induced error is sufficiently small. To identify if there are directions where a significant error occurs, it is convenient to use contour plots, as described below.

Figure 5 shows contour plots of the elevation estimation error, as determined by (11), for both case (a) and case (b) within the unambiguous region. These plots correspond to 20 GHz and the scan direction $\theta_0 = 30^\circ$, $\phi_0 = 0^\circ$. Comparing Figures 5(a) and 5(b), we note that there are some regions of radome-induced pointing error, as indicated by the red circles and arrows. The radome-induced error is below 0.05, which is sufficiently small for most applications. The size of these regions, as well as the magnitude of the pointing error, depends on the installation configuration and will be more significant for low-quality radomes. Note that the estimation error is usually smaller when the target is located close to the scan direction, i.e. centered in the main lobe of the sum pattern.

4 Conclusions

This paper presents a general method to determine installation errors on the monopulse DOA estimation for four-quadrant monopulse arrays. By using the IEPs, we compute the installation errors according to (11)-(12). By analyzing the data generated using this method, the effective coverage for an antenna can be determined with respect to the installation configuration. Regions with poor DOA estimation accuracy can then be identified, and related to causes such as reflections in the radome or the platform. Representative results were presented for two investigated cases. The presented method is general and can be used for any installation configuration on a platform, as long as the corresponding IEPs can be computed.

5 Acknowledgements

This work was supported by ChaseOn in project iAA.

References

[1] U. Nickel, "Overview of generalized monopulse estimation," *IEEE Aerospace and Electronic Systems Magazine*, vol. 21, no. 6, pp. 27–56, June 2006.

[2] S. M. Sherman and D. K. Barton, *Monopulse principles and techniques*. Artech House, 2011.

[3] B. Petersson, *Modeling of a Retrodirective Channel With Active Antenna Arrays for Cross-Eye Jamming*. Licentiate thesis, KTH Royal Institute of Technology, 2017.

[4] D. Burks, E. Graf, and M. Fahey, "A high-frequency analysis of radome-induced radar pointing error," *IEEE Transactions on Antennas and Propagation*, vol. 30, no. 5, pp. 947–955, 1982.

[5] H. Frid and B. L. G. Jonsson, "Compensation of radome effects in small airborne monopulse arrays by convex optimization," in *European Conference on Antennas and Propagation (EuCAP)*. IEEE, 2018.

[6] J. Malmström, H. Holter, and B. L. G. Jonsson, "On mutual coupling and coupling paths between antennas using the reaction theorem," *IEEE Transactions on Electromagnetic Compatibility*, vol. PP, no. 99, pp. 1–4, 2017.

[7] H. Frid, H. Holter, and B. L. G. Jonsson, "An approximate method for calculating the near-field mutual coupling between line-of-sight antennas on vehicles," *IEEE Trans. Antennas Propag.*, vol. 63, no. 9, pp. 4132–4138, 2015.

[8] R. A. Kipp and I. Capoglu, "Extending shooting-and-bouncing rays method with uniform theory of diffraction for installed antennas," in *Antennas and Propagation Society International Symposium (APSURSI), 2014 IEEE*. IEEE, 2014, pp. 2198–2199.

[9] B. Toland, "Self-guarding monopulse antenna," Jan. 10 2001, eP Patent App. EP20,000,114,632. [Online]. Available: https://www.google.com/patents/EP1067396A2?cl=en